

The impact of dark matter decays and annihilations on the formation of the first structures

E. Ripamonti¹, M. Mapelli², A. Ferrara²

¹*Kapteyn Astronomical Institute, University of Groningen, Postbus 800, 9700 AV, Groningen, The Netherlands; ripa@astro.rug.nl*

²*SISSA, International School for Advanced Studies, Via Beirut 4, 34100, Trieste, Italy*

17 May 2018

ABSTRACT

We derive the effects of dark matter (DM) decays and annihilations on structure formation. We consider moderately massive DM particles (sterile neutrinos and light DM), as they are expected to give the maximum contribution to heating and reionization. The energy injection from DM decays and annihilations produces both an enhancement in the abundance of coolants (H_2 and HD) and an increase of gas temperature. We find that for all the considered DM models the critical halo mass for collapse, m_{crit} , is generally higher than in the unperturbed case. However, the variation of m_{crit} is small. In the most extreme cases, i.e. considering light DM annihilations (decays) and halos virializing at redshift $z_{vir} > 30$ ($z_{vir} \sim 10$), m_{crit} increases by a factor ~ 4 (~ 2). In the case of annihilations the variations of m_{crit} are also sensitive to the assumed profile of the DM halo. Furthermore, we note that the fraction of gas which is retained inside the halo can be substantially reduced (to ≈ 40 per cent of the cosmic value), especially in the smallest halos, as a consequence of the energy injection by DM decays and annihilations.

Key words: galaxies: formation - cosmology: theory - dark matter - neutrinos

1 INTRODUCTION

One of the fundamental questions concerning the formation of first structures is the minimum halo mass (critical mass, m_{crit}) for collapse at a given redshift (Silk 1977; Rees & Ostriker 1977; White & Rees 1978; Couchman 1985; Couchman & Rees 1986; de Araujo & Opher 1988, 1991; Haiman, Thoul & Loeb 1996).

Tegmark et al. (1997; T97) thoroughly addressed such question, pointing out how m_{crit} crucially depends on the abundance of H_2 , the main coolant present in the metal free Universe. Subsequent studies (Abel et al. 1998; Fuller & Couchman 2000; Galli & Palla 1998, 2002; Ripamonti 2006) refined the model of T97, accounting also for minor effects, such as the cooling induced by HD molecules.

The production of molecules and m_{crit} are sensitive to any physical process which can release energy in the intergalactic medium (IGM). In fact, the injection of energy in the IGM can either delay the collapse of first halos (because of the increased gas temperature, or of photodissociation of molecules) or favour structure formation (because of the enhancement in the abundance of free electrons, which act as catalysts for the formation of molecules).

For this reason, it is crucial to understand the influence of reionization sources on structure formation. Many studies have shown that massive metal free stars are efficient in

dissociating H_2 molecules, quenching star formation in the first halos (Haiman, Rees & Loeb 1997; Ciardi, Ferrara & Abel 2000; Ciardi et al. 2000; Haiman, Abel & Rees 2000; Ricotti, Gnedin & Shull 2002; Yoshida et al. 2003). Intermediate mass black holes, produced by the collapse of first stars, are thought to efficiently re-heat the IGM, increasing m_{crit} and reducing star formation in the smaller mass halos (Ricotti & Ostriker 2004; Ricotti, Ostriker & Gnedin 2005; Zaroubi et al. 2006).

Also particle decays and annihilations can be sources of partial reionization and heating (see Mapelli, Ferrara & Pierpaoli 2006 and references therein), and could influence structure formation. For example, Shchekinov & Vasiliev (2004) investigated the possible effect on m_{crit} due to ultra-high energy cosmic rays (UHECRs) emitted by particles decaying in the early Universe. Biermann & Kusenko (2006) considered the impact on structure formation due to sterile neutrino decays. Both these studies found a substantial enhancement on the abundance of molecular coolants (H_2 and/or HD). However, they neglected the possible increase of gas temperature due to UHECRs or decays, respectively.

More recently, Stasielak, Biermann & Kusenko (2006) evaluated the effect of sterile neutrino decays accounting also for the heating of the gas. However, their single-zone model

is likely to oversimplify the crucial behaviour of gas density during the halo collapse.

In this paper, we consider the influence of dark matter (DM) decays and annihilations on structure formation, taking into account variations induced both in the chemical and in the thermal evolution of the IGM and of the gas inside halos. Furthermore, we substitute the single-zone models, which are commonly adopted in previous papers (Haiman et al. 1996 is an important exception), with more sophisticated 1-D simulations. We focus on relatively low mass DM particles, such as sterile neutrinos and light DM (LDM), as their effect on the IGM is expected to be much more important than that of heavier ($\gtrsim 100$ MeV) DM particles (Mapelli et al. 2006).

Sterile neutrinos are expected to decay into active neutrinos and keV-photons (Dolgov 2002), while LDM can either decay or annihilate producing electron-positron pairs (Boehm et al. 2004; Hooper & Wang 2004; Picciotto & Pospelov 2005; Ascasibar et al. 2006). keV-photons interact with the IGM both via Compton scattering and photo-ionization; instead, the electron-positron pairs undergo inverse Compton scattering, collisional ionizations, and positron annihilations (Zdziarski & Svensson 1989; Chen & Kamionkowski 2004; Ripamonti, Mapelli & Ferrara 2006, hereafter RMF06). RMF06 derived the fraction $f_{abs}(z)$ of energy emitted by sterile neutrino decays and LDM decays or annihilations which is effectively absorbed by the IGM through these processes. In this paper, we adopt the fits of $f_{abs}(z)$ given by RMF06.

In Section 2 we describe the hydro-dynamical code used to derive m_{crit} and the DM models which we adopt. In Section 3 we discuss the effect of DM decays and annihilations on the chemical and thermal evolution of the IGM, giving an estimate of the Jeans mass. In Section 4 we describe the chemical and thermal evolution of the gas inside the halos, deriving m_{crit} . In the discussion (Section 5) we address various points, such as the variations in the baryonic mass fraction inside the halos induced by DM decays/annihilations and the influence of the concentration of the DM profile.

We adopt the best-fit cosmological parameters after the 3-yr WMAP results (Spergel et al. 2006), i.e. $\Omega_b = 0.042$, $\Omega_M = 0.24$, $\Omega_{DM} \equiv \Omega_M - \Omega_b = 0.198$, $\Omega_\Lambda = 0.76$, $h = 0.73$, $H_0 = 100 h \text{ km s}^{-1} \text{ Mpc}^{-1}$.

2 METHOD

2.1 The code

In order to estimate the effects of the energy injection from DM decays and annihilations, it is necessary to follow the chemical and thermal evolution of primordial gas. This can be done with single-zone models such as the one originally described in T97, or the adaptations by Shchekinov & Vasiliev (2004), and by Stasielak et al. (2006). However, this kind of models is bound to use some approximations which can be very crude. First of all, single-zone models cannot follow the density evolution of a virialized halo because of their lack of "resolution", so that it is usually assumed that after virialization the gas density in a halo is both *uniform* in space and *constant* in time. Even in the linear phase of the collapse, the top-hat model provides a reasonable description of the DM component, but it becomes a rough

approximation when the baryonic component is considered, as hydro-dynamical effects are likely to become important at scales below the Jeans or the filtering length (Peebles 1993; Gnedin 2000).

An exact description would require a 3-D simulation (such as those of Abel, Bryan & Norman 2002, and of Bromm, Coppi & Larson 2002); but it is possible to capture the basic features of the collapse phenomenon by an intermediate, time-efficient approach, e.g. by means of 1-D simulation, as they are both more accurate than single-zone models, and much faster than 3-D simulations (Haiman et al. 1996).

In this paper, we use the 1-D Lagrangian, spherically symmetric code described by Ripamonti et al. (2002), as updated in Ripamonti (2006). Such a code includes the treatment of:

- the gravitational and hydro-dynamical evolution of the gas (by means of an artificial viscosity scheme);
- the chemical evolution of 12 species (H , H^+ , H^- , H_2 , H_2^+ , D , D^+ , HD , He , He^+ , He^{++} , and e^- ; see table 1 of Ripamonti 2006 for a list of the considered reactions and of the adopted reaction rates);
- the cooling (or heating) due to a number of components, such as the compressional (adiabatic) heating, the emission and absorption of line radiation from H , H_2 and HD (accounting for the effects of the cosmic microwave background, CMB), the heating (or cooling) from the Compton scattering of CMB photons off free electrons, and the heating (or cooling) due to chemical reactions (e.g. the formation or dissociation of H_2 molecules);
- the gravitational effects of DM, according to a simple model which is based on the top-hat formalism up to the turn-around redshift, smoothly evolving into a concentrated profile after virialization (see Section 2.2 for more details).

2.2 DM profiles

The code does not include a self-consistent treatment of DM. Instead, the function $\rho_{DM}(r, z)$, describing the DM density profile and its redshift evolution, must be chosen *a priori*. Since our results might depend on this choice, we decided to study two quite different cases, which we call 'isothermal' and 'NFW' (from the profile described in Navarro, Frenk & White 1997) depending on the shape of the density profile after virialization.

In both cases the DM distribution was assumed to be spherically symmetric, and concentric with the simulated region, whose central part represents the halo which is being investigated. At any redshift a DM mass $M_{DM} = M_{halo} \Omega_{DM} / \Omega_M$ is assumed to be within the truncation radius

$$R_{tr}(z) = \begin{cases} \left(\frac{3}{4\pi} \frac{M_{DM}}{\rho_{TH}(z)} \right)^{1/3} & \text{if } z \geq z_{ta} \\ R_{vir} \left[2 - \frac{t(z)}{t(z_{vir}) - t(z_{ta})} \right] & \text{if } z_{ta} > z \geq z_{vir} \\ R_{vir} & \text{if } z < z_{vir} \end{cases} \quad (1)$$

where $t(z)$ is the time corresponding to redshift z , and z_{vir} , R_{vir} and $\rho_{TH}(z)$ are the halo virialization and turn-around redshifts, its virial radius, and the DM density inside the halo at $z > z_{ta}$ (as derived from the evolution of a simple *top-hat* fluctuation; see e.g. Padmanabhan 1993, or T97),

respectively. The exact definition of these quantities can be found in Ripamonti 2006.

The isothermal and NFW assumptions differ only after the halo virialization ($z < z_{\text{vir}}$); both of them refer to a static DM profile. In the isothermal case

$$\rho_{\text{DM}}(r, z) = \begin{cases} \rho_{\text{core}} & \text{if } r \leq R_{\text{core}}; \\ \rho_{\text{core}}(r/R_{\text{core}})^{-2} & \text{if } R_{\text{core}} \leq r \leq R_{\text{tr}}; \\ \rho_0 \Omega_{\text{DM}}(1+z)^3 & \text{if } r > R_{\text{tr}}; \end{cases} \quad (2)$$

instead, in the NFW case the DM density profile is chosen to be

$$\rho_{\text{DM}}(r, z) = \begin{cases} \frac{\rho_{\text{NFW}}}{(r/R_{\text{core}})(1+r/R_{\text{core}})^2} & \text{if } r \leq R_{\text{tr}}; \\ \rho_0 \Omega_{\text{DM}}(1+z)^3 & \text{if } r > R_{\text{tr}}; \end{cases} \quad (3)$$

where $\rho_0 \simeq 1.88 \times 10^{-29} h^2 \text{ g cm}^{-3}$ is the critical density of the Universe at present. In both cases $R_{\text{core}} = \xi R_{\text{vir}}$, where $\xi = 0.1$ is a parameter (cfr. Hernquist 1993, and Burkert 1995 for the choice of its value; in the NFW case ξ the inverse of the more commonly uses concentration parameter), and the densities ρ_{core} and ρ_{NFW} can be found by requiring the DM mass within R_{tr} to be equal to M_{DM} .

At $z > z_{\text{vir}}$ both the isothermal and NFW case assume the DM density profile described by equation 2. However, at such redshift the profile is not static, because the core radius is evolved with redshift

$$R_{\text{core}}(z) = \begin{cases} R_{\text{tr}}(z) & \text{if } z \geq z_{\text{ta}} \\ R_{\text{vir}} \left[2 - \frac{(2-\xi) t(z)}{t(z_{\text{vir}}) - t(z_{\text{ta}})} \right] & \text{if } z_{\text{ta}} > z \geq z_{\text{vir}} \end{cases} \quad (4)$$

Such a choice combines the behaviour of a *top-hat* fluctuation (the density inside R_{tr} is assumed to be uniform until the turn-around) with a transition to the final density profiles.

We only considered the case $\xi = 0.1$ (i.e. concentration 10 for the NFW profile), instead of varying ξ , because the differences between the isothermal and NFW cases are quite relevant even with the same value of ξ . In fact, the NFW case is representative of concentrated halos, whereas the isothermal case is representative of relatively shallow potentials.

However, it is important to note that the flat central profile of the isothermal case helps to ensure that the behaviour we observe near the centre is due to the self-gravity and hydrodynamics of the *simulated* gas, rather than to the *assumed* DM profile.

2.3 Treatment of the DM energy injection

The above code was modified in order to include the effects of the energy injection from DM decays/annihilations on both the chemical and thermal evolution of the gas.

The gas can be heated, excited and ionized by the energy input due to DM decays/annihilations. It is important to note that the fraction of the absorbed energy going into each one of these components is quite unrelated to how the energy was deposited in the IGM at the first step. For example, if a keV a photon ionizes an atom, the resulting electron will generate a cascade of collisions, and the energy of the photon will go not only into ionizations, but also into excitations and heating.

Thus, given the energy injection per baryon from DM

Table 1. List of chemical reactions stimulated by the DM energy injection.

| Species | Reaction | Threshold |
|----------------|--|-----------|
| H | $\text{H} \rightarrow \text{H}^+ + e^-$ | 13.6 eV |
| He | $\text{He} \rightarrow \text{He}^+ + e^-$ | 24.6 eV |
| He^+ | $\text{He}^+ \rightarrow \text{He}^{++} + e^-$ | 54.4 eV |
| D | $\text{D} \rightarrow \text{D}^+ + e^-$ | 13.6 eV |
| H_2 | $\text{H}_2 \rightarrow \text{H} + \text{H}$ | 4.48 eV |
| HD | $\text{HD} \rightarrow \text{H} + \text{D}$ | 4.51 eV |
| H_2^+ | $\text{H}_2^+ \rightarrow \text{H} + \text{H}^+$ | 2.65 eV |

decays and annihilations, $\epsilon(z)$ (described in Section 2.4), we split it into an heating and ionization component¹

$$\epsilon_{\text{heat}}(z) = \tilde{C}[1 - (1 - x(z))^{\tilde{a}}]^{\tilde{b}} \epsilon(z) \quad (5)$$

$$\epsilon_{\text{ion}}(z) = \frac{1 - x(z)}{3} \epsilon(z), \quad (6)$$

where $x(z)$ is the ionization fraction. In the first equation we are using the fit to the results of Shull & Van Steenberg (1985) which is provided in their paper (with $\tilde{C} = 0.9971$, $\tilde{a} = 0.2663$, and $\tilde{b} = 1.3163$), while in the second equation we are using the fit to the same results given by Chen & Kamionkowski (2004).

The heating component is simply added to the equations describing the thermal state of the gas. Instead, the ionization component is further split between H, He, He^+ , D, H_2 , HD and H_2^+ , according to their number abundance:

$$\epsilon_i(z) = \frac{\tilde{N}_i}{\sum_{j \in (H, He, He^+, D, H_2, HD, H_2^+)} \tilde{N}_j} \epsilon_{\text{ion}}(z) \quad (7)$$

where the indices i and j indicate chemical species, and $\tilde{N}_i \equiv N_i$ if the species i is atomic, or as $\tilde{N}_i \equiv 2N_i$ if the species i is molecular; N_i is the number density (per unit volume) of the chemical species i . In principle, the terms in the sum above should be weighted by the cross-section for each species. However both the cross-section and the energy spectrum are too complex to be implemented in our simple calculations. In particular, the energy spectrum is expected to be the result of a cascade (Shull & Van Steenberg 1985). The error in neglecting these factors is quite small, as m_{crit} is more sensitive to the temperature increase than to the chemistry (see Section 4).

The quantity ϵ_i approximates the energy which is absorbed by chemical reactions dissociating the species i , and is translated into a reaction rate (number of reactions per particle per unit time) through a division by the energy threshold $E_{\text{th},i}$ of the considered reaction. The list of the reactions and of the energy thresholds is given in Table 1.

We neglect the absorption of ionization energy by H^+ , He^{++} , D^+ and e^- , because these species cannot be ionized further. We also neglect the ionization energy absorption by H^- because the energy threshold for the transformation of

¹ The sum of these two components is less than $\epsilon(z)$, as a significant fraction of the injected energy goes in atomic/molecular excitations and does not affect the chemical or thermal state of the gas.

H^- into H is negative, and cannot be treated with our simple formalism. However the number abundance of H^- is always very small, and the number of dissociations induced by DM decays/annihilations is likely to be negligible.

2.4 DM models

We apply this formalism to two different DM candidates, i.e. sterile neutrinos and LDM. Sterile neutrinos are one of the most popular warm DM (WDM) candidates (Colombi, Dodelson & Widrow 1996; Sommer-Larsen & Dolgov 2001; Bode, Ostriker & Turok 2001). They can decay via different channels (Dolgov 2002; Hansen & Haiman 2004). In this paper we are interested in the radiative decay, i.e. the decay of a sterile neutrino into a photon and an active neutrino, because of its direct impact on the IGM (Mapelli & Ferrara 2005; Mapelli et al. 2006). The photon produced in the decay interacts with the IGM both via Compton scattering and photo-ionization (RMF06).

LDM particles have recently become of interest, because they provide a viable explanation for the detected 511-keV excess from the Galactic centre (Boehm et al. 2004; Knöldlseder et al. 2005). If they are source of the 511-keV excess, then their maximum allowed mass m_{LDM} should be 20 MeV, not to overproduce detectable gamma rays via internal Bremsstrahlung (Beacom, Bell & Bertone 2004). If we consider also the production of gamma rays for inflight annihilation of the positrons, this upper limit might become ~ 3 MeV (Beacom & Yüksel 2006).

LDM can either decay or annihilate, producing photons, neutrinos and pairs. In this paper we consider both LDM decays and annihilations, but we restrict their treatment to the case where the product particles are $e^+ - e^-$ pairs. In fact, in the case of pair production the impact of LDM on the IGM is maximum (RMF06). The $e^+ - e^-$ pairs are expected to interact with the IGM via inverse Compton scattering, collisional ionization and positron annihilation (RMF06).

2.4.1 The energy input from the “background”

We first consider the energy injected in the general IGM after cosmic DM decays/annihilations.

Both in the case of sterile neutrinos and of LDM, the rate of energy transfer (per baryon) to the IGM because of this “background” contribution can be written as:

$$\epsilon_{bkg}(z) = f_{abs}(z) \dot{n}_{\text{DM}}(z) m_{\text{DM}} c^2, \quad (8)$$

where m_{DM} is the mass of a DM particle and c is the speed of light. The energy absorbed fraction, $f_{abs}(z)$, has been derived in RMF06; $\dot{n}_{\text{DM}}(z)$ is the decrease rate of the number of DM particles per baryon.

In the case of DM decays, $\dot{n}_{\text{DM}}(z)$ is given by

$$\dot{n}_{\text{DM}}(z) \simeq \frac{n_{\text{DM},0}}{\tau_{\text{DM}}}, \quad (9)$$

where $n_{\text{DM},0}$ and τ_{DM} are the current number of DM particles per baryon and the lifetime of DM particles, respectively. τ_{DM} is assumed to be much longer than the present value of the Hubble time, as is the case for all the models we are considering.

For the annihilations:

$$\dot{n}_{\text{DM}}(z) \simeq \frac{1}{2} n_{\text{DM},0}^2 N_b(0) \langle \sigma v \rangle (1+z)^3, \quad (10)$$

where $N_b(0) = 2.5 \times 10^{-7} \text{ g cm}^{-3}$ is the current baryon number density (Spergel et al. 2006), and $\langle \sigma v \rangle$ is the thermally averaged DM annihilation cross-section.

Both for sterile neutrinos and LDM, the values of $n_{\text{DM},0}$, τ_{DM} and $\langle \sigma v \rangle$ adopted in this paper are the same reported in RMF06; for convenience, they are listed in Table 2.

2.4.2 The “local” energy input

In addition to the background energy injection discussed above, the baryons inside a halo absorb extra energy from the additional decays/annihilations of overdense halo DM. In the case of decays the total excess energy “produced” inside the halo is

$$E_{loc}(z) = \frac{4\pi N_b(0)(1+z)^3 m_{\text{DM}} c^2}{\tau_{\text{DM}}} \times \int_0^{R_{tr}(z)} dr r^2 [n_{\text{DM}}(r, z) - n_{\text{DM},0}], \quad (11)$$

and in the case of annihilations

$$E_{loc}(z) = 4\pi [N_b(0)(1+z)^3]^2 m_{\text{DM}} c^2 \langle \sigma v \rangle \times \int_0^{R_{tr}(z)} dr \frac{1}{2} r^2 [n_{\text{DM}}^2(r, z) - n_{\text{DM},0}^2(z)], \quad (12)$$

where $n_{\text{DM}}(r, z) = \rho_{\text{DM}}(r, z) / [m_{\text{DM}} N_b(0)(1+z)^3]$ is the number of DM particles per baryon at redshift z and at a distance r from the centre of the halo.

Then, we compute the baryon column density Σ_b from the halo centre to the truncation radius, and find the fraction of the energy E_{loc} which is absorbed by such a column density, f_{loc} . If the DM produces photons of energy E_γ ,

$$f_{loc} = \Sigma_b \left[\sigma_{He+H}(E_\gamma) + \sigma_T \frac{E_\gamma}{m_e c^2} g \left(\frac{E_\gamma}{m_e c^2} \right) \right] \quad (13)$$

where $\sigma_{He+H}(E)$ is the photo-ionization cross section (see Zdziarski & Svensson 1989; RMF06), σ_T is the Thomson cross section, and the function g is defined in equation 4.9 of Zdziarski & Svensson (1989). Instead, if the DM produces electron-positron pairs with Lorentz factor γ (and energy $E = \gamma m_e c^2$),

$$f_{loc} = \frac{\Sigma_b}{c N_b(0)(1+z)^3} \phi_{e,ion}(z, E) + \frac{R_{tr}(z)}{c} \phi_{e,com}(z, E) \quad (14)$$

where $\phi_{e,ion}(z, E)$ and $\phi_{e,com}(z, E)$ give the fraction of the energy of an electron/positron which is absorbed per unit time by the IGM, because of collisional ionizations and of Compton scattering of CMB photons, respectively. Such functions are given by equations 14-15, and 16-18 of RMF06.

We then assume that all the baryons inside the halo absorb the same amount of energy from this local contribution. So, the “local” energy deposition in each baryon within the truncation radius $R_{tr}(z)$ is

$$\epsilon_{loc}(z, r) = E_{loc} f_{loc} \frac{M_{\text{gas}}[R_{tr}(z)]}{m_H} \quad (15)$$

where $M_{\text{gas}}(R_{tr})$ is the mass of the gas inside the truncation radius, and m_H is the mass of an H atom. Instead, for baryons at a distance larger than $R_{tr}(z)$ from the centre of the halo we assume $\epsilon_{loc}(z, r) = 0$.

Table 2. List of the main characteristics of the considered DM models. In particular, from the leftmost to the rightmost column: DM model, $n_{\text{DM},0}$, τ_{DM} (if decaying particle), $\langle \sigma v \rangle$ (if annihilating), comoving free-streaming lengths ($\lambda_{\text{FS},n}$ and $\lambda_{\text{FS},i}$) and the associated mass scale. λ_{FS} is taken to be the maximum between $\lambda_{\text{FS},n}$ and $\lambda_{\text{FS},i}$.

| DM model | $n_{\text{DM},0}/10^3$ | $\tau_{\text{DM}}/(10^{27} \text{ s})$ | $\langle \sigma v \rangle/(10^{-29} \text{ cm}^3 \text{ s}^{-1})$ | $\lambda_{\text{FS},n}(\text{pc})$ | $\lambda_{\text{FS},i}(\text{pc})$ | $M_{\text{FS}}(M_{\odot})$ |
|---------------------------|------------------------|--|---|------------------------------------|------------------------------------|----------------------------|
| ν 4 keV (decaying) | 1176 | 2.96 | — | 3×10^5 | 60 | 5×10^8 |
| ν 15 keV (decaying) | 314 | 1.98 | — | 8×10^4 | 35 | 1×10^7 |
| ν 25 keV (decaying) | 188 | 0.097 | — | 4.8×10^4 | 25 | 2×10^6 |
| LDM 3 MeV (decaying) | 1.49 | 1.2 | — | 2.2 | < 0.1 | 2×10^{-7} |
| LDM 10 MeV (decaying) | 0.446 | 4.0 | — | 0.5 | < 0.1 | 3×10^{-8} |
| LDM 1 MeV (annihilating) | 4.46 | — | 4 | 9.5 | 300 | 0.5 |
| LDM 3 MeV (annihilating) | 1.49 | — | 12 | 2.2 | 100 | 0.02 |
| LDM 10 MeV (annihilating) | 0.446 | — | 24 | 0.5 | 30 | 5×10^{-4} |

The total energy input per baryon from DM decays/annihilations is then

$$\epsilon(r, z) = \epsilon_{bkg}(z) + \epsilon_{loc}(r, z). \quad (16)$$

2.5 The free-streaming/damping lengths

We need to take into account that small DM fluctuations might be washed out by damping mechanisms, and in particular by free-streaming (see e.g. Padmanabhan 1993; Sommer-Larsen & Dolgov 2001; Boehm et al. 2005).

The free-streaming scale depends on the considered particle, and on the strength of its interactions. If such interactions are negligible, the comoving free-streaming length is

$$\lambda_{\text{FS},n} \simeq \begin{cases} 0.3 \left(\frac{m_{\text{DM}} c^2}{4 \text{ keV}} \right)^{-1} \left(\frac{\langle p c / (k_B T) \rangle}{3.15} \right) \text{ Mpc} & \text{for neutrinos} \\ 0.20 (\Omega_{\text{DM}} h^2)^{1/3} \left(\frac{m_{\text{DM}} c^2}{1 \text{ keV}} \right)^{-4/3} \text{ Mpc} & \text{for LDM,} \end{cases} \quad (17)$$

where m_{DM} is the mass of the considered DM particle, p and T are the modulus of the proper momentum and the temperature of the particle, respectively. The above expressions are derived from Abazajian, Fuller & Patel (2001), and from Boehm et al. (2005), respectively.

However, if the DM particle interacts at a non negligible rate, the comoving free-streaming length is (Boehm et al. 2005; Boehm & Schaeffer 2005)

$$\lambda_{\text{FS},i} = 0.3 \left(\frac{m_{\text{DM}} c^2}{1 \text{ MeV}} \right)^{-1/2} \left(\frac{\tilde{\Gamma}_{\text{dec,DM}}}{6 \times 10^{-24} \text{ s}^{-1}} \right)^{1/2} \text{ Mpc} \quad (18)$$

with

$$\tilde{\Gamma}_{\text{dec,DM}} = \Gamma_{\text{DM}}(z_{\text{dec}})(1 + z_{\text{dec}})^{-3}, \quad (19)$$

where $\Gamma_{\text{DM}}(z_{\text{dec}})$ is the DM interaction rate at its decoupling redshift z_{dec} .

In the case of decaying particles, we assume that this rate is simply the inverse of the present lifetimes of DM particles; so, $\Gamma_{\text{DM}}(z_{\text{dec}}) < 10^{-24} \text{ s}^{-1}$ in all the cases we are considering (cfr. Table 2). Since $z_{\text{dec}} \gg 10^3$, equations (17) and (18) imply that $\lambda_{\text{FS},i} \ll \lambda_{\text{FS},n}$; so, for decaying particles we will use a free-streaming scale $\lambda_{\text{FS}} = \lambda_{\text{FS},n}$.

Instead, when annihilating particles are considered, the interaction rate is $\Gamma_{\text{DM}}(z_{\text{dec}}) = \frac{1}{2} n_{\text{DM},0} N_{\text{b}}(0) \langle \sigma v \rangle_{\text{dec}} (1 + z_{\text{dec}})^3$, where $\langle \sigma v \rangle_{\text{dec}} \sim 10^{-26} \text{ cm}^3 \text{ s}^{-1}$ (see, for example,

Ascasibar et al. 2006) is the thermally averaged annihilation cross section at the epoch of decoupling². Then, in the case of annihilating particles, $\lambda_{\text{FS},i} \gg \lambda_{\text{FS},n}$, and we must assume $\lambda_{\text{FS}} = \lambda_{\text{FS},i}$. In Table 2 we give the detailed list of the free-streaming lengths for each DM model. The same table also lists the free-streaming mass scale

$$M_{\text{FS}} = \frac{4\pi}{3} \left(\frac{\lambda_{\text{FS}}}{2} \right)^3 \rho_0 \Omega_{\text{M}} h^2. \quad (20)$$

Damping erases fluctuations on scales smaller than λ_{FS} . Thus, objects of mass $\lesssim M_{\text{FS}}$ are unlikely to form, unless the small scale power spectrum is regenerated by non-linear effects at low redshift (see Boehm et al. 2005; however, this regeneration appears to take place at $z \sim 2$, which is much later than the epoch we are considering). To introduce corrections for this effect in our models is beyond the purposes of this paper.

Damping might also affect the density profile of halos, erasing cusps on scales $\lesssim \lambda_{\text{FS}}$. The values of λ_{FS} and M_{FS} listed in Table 2 show that this effect of damping can be important only for sterile neutrinos. In the case of isothermal density profiles, we account for it adopting the following correction. If the core radius $R_{\text{core}}(z)$ (equation 4) is smaller than $\lambda_{\text{FS}}/2$, we increase its value to $R_{\text{core,new}}(z) = \min(R_{\text{tr}}(z), \lambda_{\text{FS}}/2)$. Instead, in the case of simulations with NFW density profile we do not introduce this correction, because these simulations are intended to explore the effects of high concentration (see Section 4.2).

2.6 The simulations

Our code was used to run a large number of simulations, in order to explore a wide range of the $z_{\text{vir}} - M_{\text{halo}}$ parameter space: we considered halo masses in the range $10^4 - 10^7 M_{\odot}$, and virialization redshifts between 10 and 100.

We actually simulate a mass which is 1000 times higher than that of the collapsing halo, in order to include in the

² For annihilating particles, a third scale length might be considered, i.e. the mixed damping length λ_{md} (Boehm et al. 2003). The upper limit of λ_{md} is 6.7, 2.9 and 1.2 kpc for 1, 3 and 10 MeV LDM, respectively. These values are a factor ~ 20 larger than the corresponding $\lambda_{\text{FS},i}$; but our conclusions about m_{crit} (see Section 4) are not significantly affected, because M_{FS} is still smaller than the mass range we are considering.

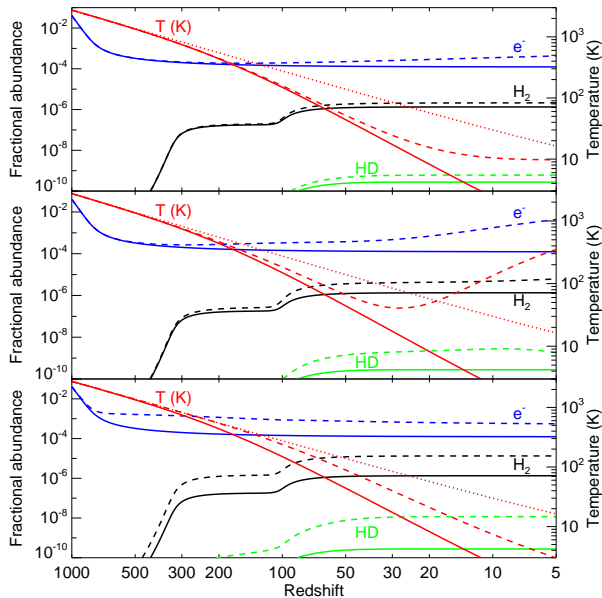


Figure 1. Effects of decaying/annihilating DM on the IGM evolution. Left axis: fractional abundances of free electrons (e^-), H_2 and HD as a function of redshift. Right axis: matter temperature as a function of redshift. Top panel: Effect of decaying sterile neutrinos of mass 25 keV (dashed line). Central panel: decaying LDM of mass 10 MeV (dashed line). Bottom panel: annihilating LDM of mass 1 MeV (dashed line). In all the panels the dotted line is the CMB temperature and the solid line represents the thermal and chemical evolution without DM decays/annihilations.

simulation a mass which is larger than the cosmological filtering mass (Gnedin 2000); otherwise, our treatment of hydrodynamics might be incorrect. The simulated object is divided in 150 shells, whose spacing was chosen so that (i) the mass of the shells smoothly increases when moving outwards, (ii) the central shell always encloses a gas mass of $\sim 0.3 M_\odot$, and (iii) the central 100 shells initially enclose a mass $\sim M_{halo}$ (including the DM).

The simulations are started at $z = 1000$, when we assume that the gas density is uniformly equal to the cosmological value (whereas the DM density profile is not perfectly uniform; see Section 2.2), the gas temperature is equal to the CMB temperature ($\simeq 2.728$ K), and adopt the chemical abundances listed in table 2 of Ripamonti 2006³.

They are stopped either when the gas density reaches the threshold $\rho/m_H = 10^5$ cm $^{-3}$, or after a time $2t(z_{vir})$ has elapsed.

Each set of simulations was repeated for each different DM decay/annihilation model, and also for the “standard” case without any energy injection from DM, which is used as a reference against which we compare our results.

³ The most important abundances listed there are the H ionization fraction (at $z = 1000$) $N_{H^+}/N_H = 0.0672$, the helium abundance $N_{He}/N_H = 0.0833$, and the deuterium abundance $N_D/N_H = 2.5 \times 10^{-5}$.

3 IGM EVOLUTION

In order to look at the influence of DM decays and annihilations upon the IGM, we have used a simplified version of our code (where the density was assumed to evolve as the cosmological value).

3.1 Chemistry and temperature

Our code follows the chemical evolution of 12 chemical species (see previous Section). Two of them, molecular hydrogen (H_2) and HD are particularly important for our purposes, because they are the main coolant of the metal free gas. In Fig. 1 we show the fractional abundances of both H_2 and HD together with the ionized fraction and the matter temperature as a function of redshift for the considered DM models.

In all the DM models, both the matter temperature and the abundance of H_2 , HD and free electrons are enhanced by DM decays/annihilations. This effect is smaller for sterile neutrinos than for LDM particles. The main difference between decays and annihilations is represented by the redshift range in which the influence of DM is important. For all the considered quantities (i.e. temperature and abundance of e^- , H_2 and HD) the energy injection from DM decays starts to be significant at redshift lower than ~ 100 . Instead, the influence of annihilations is important already at redshift ~ 900 . The annihilations represent also the case where the abundance of the two coolants is most enhanced (a factor ~ 17 for the H_2 and ~ 90 for the HD). Furthermore, the annihilations keep the matter temperature close to the CMB temperature everywhere, up to $z \sim 50 - 100$. This fact can have important consequences for experiments searching for high redshift HI 21-cm line signals (Shchekinov & Vasiliev 2006).

3.2 Jeans mass

In order to establish the influence of DM decays or annihilations on the structure formation, the key point is the following. DM decays and annihilations increase both the matter temperature and the abundance of coolants. The former effect tends to delay the formation of structures, while the latter favours an early collapse of the halos. Which of these two opposite effects is dominant? When looking at the average properties of the IGM, the most popular diagnostic is the cosmological Jeans mass, m_J (Peebles 1993):

$$m_J(T, \rho, \mu) = \frac{\pi}{6} \left(\frac{\pi k_B T}{G \mu m_H} \right)^{3/2} \rho^{-1/2} \simeq 50 M_\odot T^{3/2} \mu^{-3/2} \left(\frac{\rho}{m_H} \right)^{-1/2}, \quad (21)$$

where k_B is the Boltzmann constant, G the gravitational constant and μ the mean molecular weight.

In Fig. 2 we show the evolution of m_J . For all the considered DM models m_J is considerably increased by the effect of decays and annihilations. This means that, when the IGM is considered, the increase of the matter temperature dominates over the enhancement of the coolant abundance. For example, at $z = 10$ $m_J = 3.0 \times 10^7 M_\odot$ in the case of 10-MeV LDM decays, a factor ~ 420 higher than in the unperturbed

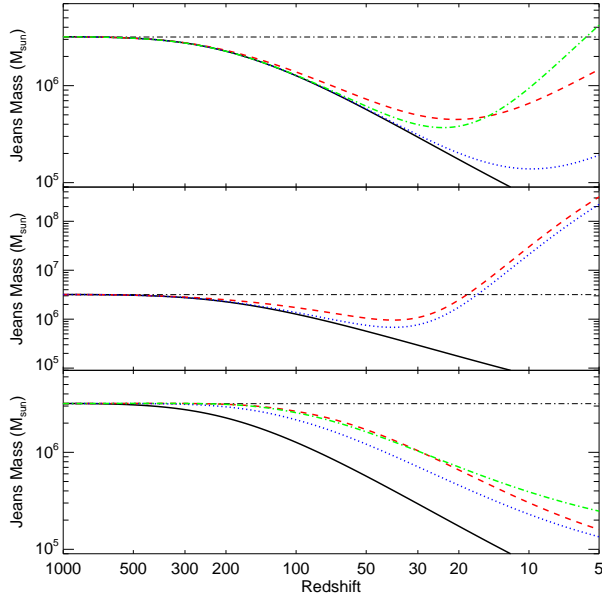


Figure 2. Jeans mass as a function of redshift. Top panel: Effect of decaying sterile neutrinos of mass 25 (dashed line), 15 (dotted) and 4 keV (dot-dashed). Central panel: Decaying LDM of mass 10 (dashed line) and 3 MeV (dotted). Bottom panel: Annihilating LDM of mass 10 (dashed line), 3 (dotted) and 1 MeV (dot-dashed). In all the panels the solid line represents the thermal and chemical evolution without DM decays/annihilations. The horizontal dot-dashed line shows the behaviour of the Jeans mass calculated by assuming that the gas temperature is always equal to the CMB temperature.

case (for which $m_J = 7.2 \times 10^4 M_\odot$). The increase of m_J is less pronounced, but nevertheless significant in the case of sterile neutrino decays ($m_J = 6.6 \times 10^5 M_\odot$ for 25-keV sterile neutrinos) and LDM annihilations ($m_J = 3.9 \times 10^5 M_\odot$ for 1-MeV LDM).

From this fact one could naively infer that DM decays and annihilations strongly delay the formation of the first structures. However, m_J refers only to the global properties of the IGM, and does not account for the non-linear evolution of collapsing halos.

4 EVOLUTION INSIDE HALOS

4.1 Chemistry and temperature

To assess the star forming ability of the first halos, it is necessary to follow their hydro-dynamical and chemical evolution. This has been done by using the code described in Section 2. Fig. 3 (Fig. 4) shows, as an example, the evolution of the most relevant properties of the gas at the centre of a $6 \times 10^5 M_\odot$ ($2 \times 10^6 M_\odot$) halo, virializing at $z_{vir} = 12$. In these figures the effects of different DM decay/annihilation scenarios are compared with the unperturbed case. For the smaller halo (Fig. 3) LDM annihilations and sterile neutrino decays delay the collapse by ~ 1 redshift units, and in the case of LDM decays this effect is even more significant: in presence of 10 MeV-LDM decays the halo has not collapsed yet after one Hubble time from virialization. Instead, for the

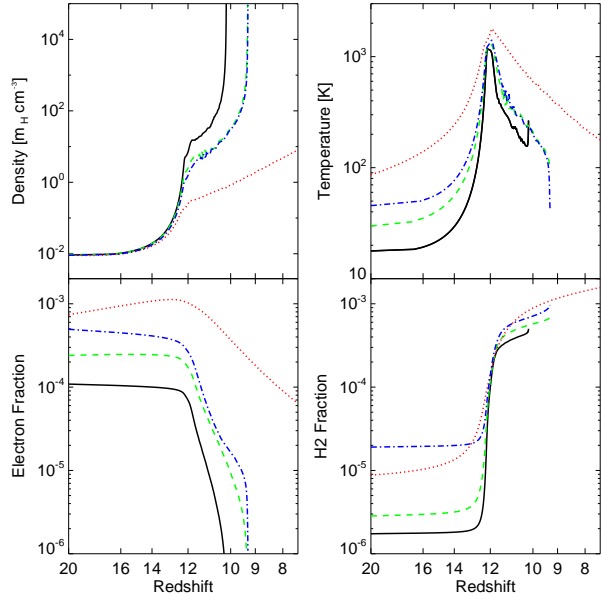


Figure 3. Evolution of the central region of a $6 \times 10^5 M_\odot$ isothermal halo virializing at $z_{vir} = 12$. From left to right and from top to bottom: density, temperature, electron abundance and H_2 abundance as function of redshift. The solid line represents the unperturbed case (i.e. without DM decays and annihilations). The dashed, dot-dashed and dotted lines account for the contribution of 25-keV sterile neutrino decays, 1-MeV LDM annihilations and 10-MeV LDM decays, respectively.

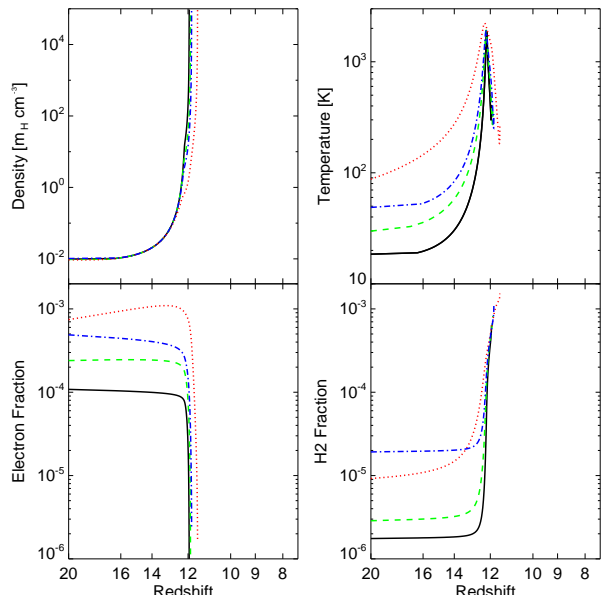


Figure 4. Evolution of the central region of a $2 \times 10^6 M_\odot$ isothermal halo virializing at $z_{vir} = 12$. From left to right and from top to bottom: density, temperature, electron abundance and H_2 abundance as function of redshift. The dashed, dot-dashed and dotted lines are the same as in Fig. 3.

larger halo (Fig. 4) the difference between the case with and without DM decays/annihilations is negligible.

It is worth to discuss in detail the gas temperature (T) and number density ($N = \rho/m_H$) evolution shown in Fig. 3. At the epoch of turn-around ($z \sim 19 - 20$) all the models have the same N ; but in the unperturbed one T is 1.5–5 times lower than in the others. This is important, because the fast increase in T and N due to the virialization process is essentially adiabatic, as it happens on a time-scale much faster than that for cooling. In the adiabatic approximation, $\Gamma_{ad} = -P dV \propto P [N^{-1} - (N + \Delta N)^{-1}]$ (where P is the gas pressure), is proportional to the initial T for any given increase in N . T and P increase faster in models "pre-heated" by DM decays/annihilations, so that the pressure gradient slowing and halting the collapse develops earlier. In fact, the phase of unimpeded collapse stops at $N \sim 10 \text{ cm}^{-3}$ for the unperturbed case, but only at $N \sim 0.3 - 3 \text{ cm}^{-3}$ for the other models. At these densities the cooling per unit mass is proportional both to the H_2 fraction and to N , so that the higher central density of the model without DM decays/annihilations largely compensates its lower H_2 abundance, i.e. the unperturbed case is the *fastest* cooling one. However, it is interesting to note that the final T is much lower for the cases where DM energy input is included, because of the enhancement of the HD fraction, which provides an efficient cooling mechanism also at $T \lesssim 200 \text{ K}$ (Ripamonti 2006).

4.2 Critical mass

Each of our simulated halos was classified as collapsing (or, equivalently, efficiently cooling) or non-collapsing (inefficiently cooling), depending on whether it reaches a maximum density larger than $10^5 m_H \text{ cm}^{-3}$ in less than a Hubble time. We define the critical mass, m_{crit} , as the minimum mass of a collapsing halo at a given virialization redshift z_{vir} .

The values of m_{crit} as a function of the virialization redshift are shown in Fig. 5 for isothermal halos, and in Fig. 6 for NFW halos. The main trend inferred from the behaviour of m_J (i.e. the delay of structure formation) is confirmed by m_{crit} . However, the influence of DM decays and annihilations on m_{crit} is much smaller than could be expected from m_J .

In the case of isothermal halos, the effects of the DM decays on m_{crit} (top and central panel) are completely negligible at high redshift and become significant only at redshift less than 20. Even for $z_{vir} = 10$ and 10-MeV decaying LDM (which has the strongest effect), m_{crit} increases only by a factor 2.

Sterile neutrinos (especially with mass of 4 keV) seem to significantly increase m_{crit} . However, this is not connected with sterile neutrinos decays; but it is mainly due to differences in the assumed DM density profile, as the free-streaming length for these WDM halos is larger than the "standard" value of the core radius ($0.1 R_{vir}$) and the "damping" correction described in Section 2.5 is important. In fact, m_{crit} is almost the same down to $z \sim 20$, if we consider (thick dot-dashed line in Fig. 5) or neglect (thin solid line) sterile neutrino decays, and the difference between these two cases is small even at lower redshift.

In the case of LDM annihilations in isothermal halos, m_{crit} is higher than in the unperturbed case for every con-

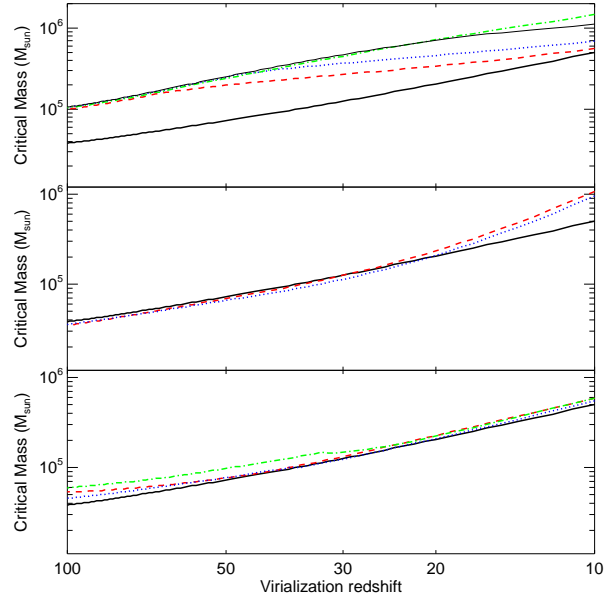


Figure 5. The critical mass as a function of the virialization redshift z_{vir} for isothermal halos. Top panel: Effect of decaying sterile neutrinos. Central: Decaying LDM. Bottom: Annihilating LDM. The lines used in the three panels are the same as in Fig. 2. The thin solid line used in the top panel represents the case of non-decaying WDM (with mass 4 keV).

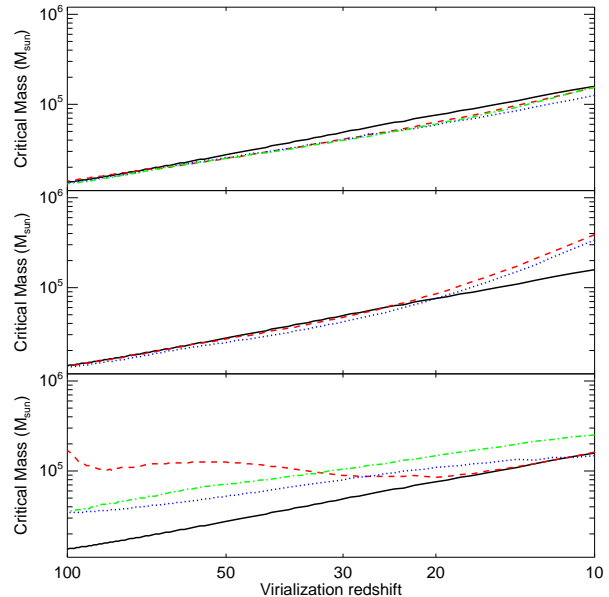


Figure 6. The critical mass as a function of the virialization redshift z_{vir} for NFW halos. The lines used in the three panels are the same as in Fig. 5.

sidered virialization redshift ($z_{vir} = 10 - 100$), confirming that the annihilations play a role even at very high z . However, the difference with respect to the unperturbed m_{crit} is always less than a factor ~ 2 .

If we assume a NFW profile for DM halos (Fig. 6), the general effect is a substantial decrease of m_{crit} (inde-

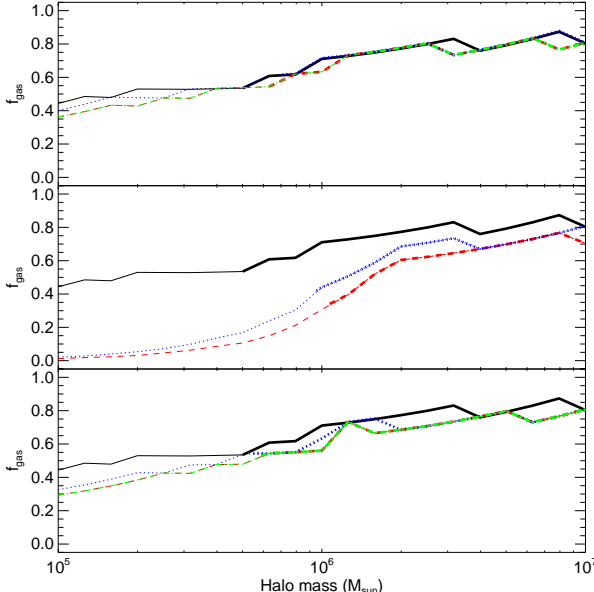


Figure 7. Halo baryonic mass fraction (see definition in equation 22) as a function of the halo mass for a fixed virialization redshift ($z_{vir} = 10$) and for an isothermal DM profile. Top panel: Effect of decaying sterile neutrinos. Central: Decaying LDM. Bottom: Annihilating LDM. The lines used in the three panels are the same as in Fig. 2. Thick (thin) lines indicate that the halo mass is larger (smaller) than m_{crit} .

pendently of DM decays/annihilations), due to the higher central densities, and the consequent stronger gravitational pull. LDM decays tend to increase m_{crit} (at $z < 20$) with respect to the unperturbed case; the increase factor is only marginally larger than in the case of isothermal halos. Sterile neutrino decays appear to slightly reduce m_{crit} with respect to the unperturbed case; but this result is unphysical, as it does not account for damping. It is worth to note that, even if we ignore damping effects and adopt the models with the highest possible concentration, the influence of sterile neutrino decays on structure formation remains very small.

Instead, in the case of LDM annihilations, m_{crit} generally increases more in NFW halos than in isothermal halos. This is due to the importance of the local contribution for annihilations (see Section 5.2).

5 DISCUSSION

5.1 Gas fraction

Why considering either m_J or m_{crit} leads to such widely different conclusions? As mentioned earlier, m_J is a rough tracer of the minimum halo mass for collapse; but it is not sensitive to the local properties of the halo. For example, to calculate m_J one has to assume that the density is uniform. On the contrary, m_{crit} depends on the evolution of the central region of the halo, where the density increases much more rapidly than in the outskirts, driving the collapse (Figs. 3 and 4). When the density becomes sufficiently high, the molecular cooling largely overcomes the heating due to DM decays/annihilations (Figs. 3 and 4). This is the reason why m_{crit} does not increase significantly in presence of DM

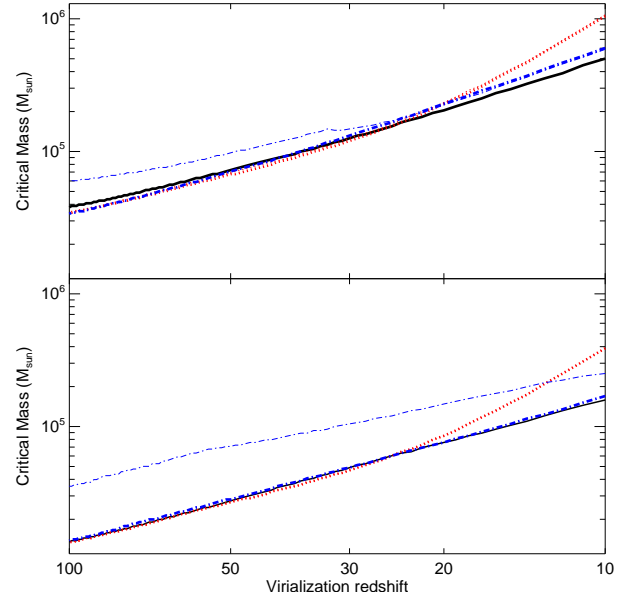


Figure 8. Evolution of m_{crit} as a function of the virialization redshift in the case without DM (solid lines), with 3-MeV LDM decays (dotted) and with 1-MeV LDM annihilations (dot-dashed). Thin (thick) lines are with (without) the local contribution of the DM inside the halo. Note that the thin dotted line is completely superimposed to the thick dotted line, because the local contribution of decaying DM is always negligible. Top panel: isothermal halos. Bottom panel: NFW halos.

decays/annihilations. Instead, m_J , which does not account for the density increase and for the consequent cooling enhancement, dramatically grows. Then, we can conclude that m_J does not provide a realistic estimate of the effects of DM decays/annihilations.

Is there any physical implication of the growth of m_J ? m_J is directly related to the global hydro-dynamical behaviour of the gas inside a halo: in halos with mass below m_J the gas pressure prevents the development of a large gas overdensity, while in more massive halos the gas accumulation should proceed almost unimpeded. If so, the mass fraction in baryons within the virial radius of a halo should be of the order of the cosmological average Ω_b/Ω_M when $M_{halo} \gtrsim m_J$, but it should be lower when $M_{halo} \lesssim m_J$. To check this hypothesis, we derive the baryonic mass fraction (f_{gas}) normalized to Ω_b/Ω_M , i.e.

$$f_{gas} = \frac{M_{gas}(R_{vir})}{M_{halo}} \frac{\Omega_M}{\Omega_b}, \quad (22)$$

where $M_{gas}(R_{vir})$ is the mass of gas within the virial radius at the final stage of each simulation; instead M_{halo} is the total mass of the halo at the beginning of the simulation.

In Fig. 7 we show f_{gas} as a function of mass inside halos virializing at redshift $z_{vir} = 10$. The comparison between the various scenarios clearly shows that the energy injection from DM decays/annihilations can substantially reduce the gas fraction inside all halos, especially the smallest ones. This is clearly related to the increase in m_J , as the largest variation in f_{gas} occurs in the LDM decay scenario, where the increase of m_J is maximum (Fig. 2).

5.2 Concentration and local contribution

In this paper we basically considered two different DM profiles: isothermal and NFW halos. These two models are comparable in terms of virial radius and main properties; but the NFW one is much more concentrated. From the comparison between Fig. 5 and Fig. 6 we have already seen that this difference has important effects on the critical mass: m_{crit} is generally much lower for a NFW than for an isothermal halo, independently of DM decays and annihilations. For decaying particles, higher concentrations lead to marginally stronger effects in delaying the formation of structures, but the effect is minimal. For annihilations this effect of high concentrations is much larger (see Figs. 5, 6 and 8).

Another significant characteristic of our model is the estimate of the local contribution due to DM decays/annihilations occurring inside the halo (see Section 2.4.2). Pointedly, the local contribution strongly depends on the DM profile. But what is the importance of the local contribution? In Fig. 8 we indicate the effect on m_{crit} of LDM decays (dotted line) and annihilations (dot-dashed), by including (thin line) or not (thick) the local contribution. In the case of DM decays the thin and thick dotted lines appear superimposed, both in the isothermal (top panel) and NFW (bottom) profile, indicating that the local contribution is always negligible for decays.

Instead, if we consider the annihilations, the case with (thin line) and without (thick) the local contribution are very different, especially for the NFW profile. If we do not include the local contribution, m_{crit} is very close to the unperturbed value. If we switch on the local contribution in the isothermal profile, m_{crit} is substantially higher (a factor ~ 2) than in the unperturbed case, at least for high virialization redshifts ($z_{vir} > 30$). Finally, if we account for the local contribution in a NFW halo, m_{crit} is always higher (a factor $\sim 2 - 4$) than in the unperturbed case (even at low virialization redshifts). This is consistent with the fact that the annihilation rate strongly depends on the local DM density.

6 CONCLUSIONS

In this paper we derived the effects of DM decays and annihilations on structure formation. We considered only moderately massive DM particles (sterile neutrinos and LDM), as they are expected to give the maximum contribution to heating and reionization (Mapelli et al. 2006). To describe the interaction between the IGM and the decay/annihilation products we followed the recipes recently derived by RMF06.

We accounted not only for the diffuse cosmological contribution to heating and ionization, but also for the local contribution due to DM decays and annihilations occurring in the halo itself. The local contribution results to be dominant in the case of DM annihilations especially for cuspy DM profiles.

The energy injection from DM decays/annihilations produces both an enhancement in the abundance of coolants (H_2 and HD) and an increase of gas temperature. We found that for all the considered DM models (sterile neutrino decays, LDM decays and annihilations) the critical halo mass for collapse, m_{crit} is often higher than in the unperturbed

case. This means that DM decays and annihilations tend to delay the formation of structures. However, the variation of m_{crit} is minimal. In the most extreme cases, i.e. considering LDM annihilations (decays) and halos virializing at redshift $z_{vir} > 30$ ($z_{vir} \sim 10$), m_{crit} increases of a factor ~ 4 (~ 2). In the case of decays, the variations of m_{crit} are almost independent from the assumed concentration of the DM halo, although higher concentrations (corresponding to smaller values of m_{crit}) seem to be associated with slightly stronger effects of the DM energy injection. The dependence on concentration is more evident in the case of annihilating particles, where higher concentrations lead to substantially larger effects. This happens because the “local” contribution is important.

In summary, the effects of DM decays and/or annihilations on structure formation are quite small, except in some extreme cases (e.g. very high concentration for annihilations). However, the energy injection from DM decays/annihilations has important consequences on the fraction of gas which is retained inside the halo. This fraction can be substantially reduced, especially in the smallest halos ($\lesssim 10^6 M_\odot$).

Finally, we point out that our results are quite different from the conclusions of Biermann & Kusenko (2006) and Stasielak et al. (2006)⁴, who suggest that sterile neutrino decays can favour the formation of first objects. The discrepancy is likely due to our more complete treatment which includes the hydrodynamics of the collapsing structures. In fact, our hydro-dynamical treatment allows to describe the detailed gas density evolution during the collapse, resulting in markedly different temperature and chemical properties with respect to those found by a simple one-zone model.

ACKNOWLEDGEMENTS

We thank S. Zaroubi, C. Watson, A. Kusenko, P. Biermann and J. Stasielak for useful discussions. We also acknowledge the referee for a critical reading of the paper. The three authors thank both SISSA/ISAS and the Kapteyn Institute for mutual hospitality during the preparation of this paper. ER gratefully acknowledges support from the Netherlands Organization for Scientific Research (NWO) under project number 436016.

REFERENCES

- Abazajian K., Fuller G. M., Patel M., 2001, Phys. Rev. D, 64b, 3501
- Abel T., Anninos P., Norman M. L., Zhang Y., 1998, ApJ, 508, 518
- Abel T., Bryan G. L., Norman M. L., 2002, Sci, 295, 93
- Ascasibar Y., Jean P., Boehm C., Knöldlseder J., 2006, MNRAS, 368, 1695
- Beacom J. F., Bell N. F., Bertone G., 2005, Phys. Rev. Lett., 94q, 1301
- Beacom J. F., Yüksel H., 2006, Phys. Rev. Lett., 97g, 1102
- Biermann P. L., Kusenko A., 2006, Phys. Rev. Lett., 96L, 1301

⁴ Biermann & Kusenko (2006) and Stasielak et al. (2006) do not calculate the critical mass m_{crit} . So, it is quite difficult to make a quantitative comparison between their results and ours.

Bode P., Ostriker J. P., Turok N., 2001, ApJ, 556, 93

Boehm C., Hooper D., Silk J., Cassé M., Paul J., 2004, Phys. Rev. Lett., 92j, 1301

Boehm C., Mathis H., Devriendt J., Silk J., 2003, astro-ph/0309652

Boehm C., Mathis H., Devriendt J., Silk J., 2005, MNRAS, 360, 282

Boehm C., Schaeffer R., 2005, A&A, 438, 419

Bromm V., Coppi P. S., Larson R. B., 2002, ApJ, 564, 23

Burkert A., 1995, ApJ, 447, L25

Chen X., Kamionkowski M., 2004, Phys. Rev. D, 70d, 3502

Ciardi B., Ferrara A., Abel T., 2000, ApJ, 533, 594

Ciardi B., Ferrara A., Governato F., Jenkins A., 2000, MNRAS, 314, 611

Colombi S., Dodelson S., Widrow L. M., 1996, ApJ, 458, 1

Couchman H.M.P., 1985, MNRAS, 214, 137

Couchman H.M.P., Rees M.J., 1986, MNRAS, 221, 53

de Araujo J.C.N., Opher R., 1988, MNRAS, 231, 923

de Araujo J.C.N., Opher R., 1991, ApJ, 379, 461

Dolgov A. D., 2002, Phys. Rept., 370, 333 (hep-ph/0202122)

Fuller T. M., Couchman H.M.P., 2000, ApJ, 544, 6

Galli D., Palla F., 1998, A&A, 335, 403

Galli D., Palla F., 2002, P&SS, 50, 1197

Gnedin N. Y., 2000, ApJ, 542, 535

Haiman Z., Abel T., Rees M. J., 2000, ApJ, 534, 11

Haiman Z., Rees M. J., Loeb A., 1997, ApJ, 476, 458

Haiman Z., Thoul A.A., Loeb A., 1996, ApJ 464, 523

Hansen S. H., Haiman Z., 2004, ApJ, 600, 26

Hernquist L., 1993, ApJS, 86, 389

Hooper D., Wang L.-T., 2004, Phys. Rev. D, 70f, 3506

Knödlseder J. et al., 2005, A&A, 441, 513

Mapelli M., Ferrara A., 2005, MNRAS, 364, 2

Mapelli M., Ferrara A. & Pierpaoli E., 2006, MNRAS, 369, 1719

Peebles P. J. E., 1993, *Principles of physical cosmology*, Princeton University Press, Princeton

Picciotto C., Pospelov M., 2005, Phys. Lett. B, 605, 15

Rees M.J., Ostriker J.P., 1977, MNRAS, 179, 541

Ricotti M., Gnedin N. Y., Shull J.M., 2002, ApJ, 575, 49

Ricotti M., Ostriker J. P., 2004, MNRAS, 352, 547

Ricotti M., Ostriker J. P., Gnedin N. Y., 2005, MNRAS, 357, 207

Ripamonti E., 2006, MNRAS, submitted

Ripamonti E., Haardt F., Ferrara A., Colpi M., 2002, MNRAS, 334, 401

Ripamonti E., Mapelli M., Ferrara A., 2006, MNRAS, accepted (astro-ph/0606482) [RMF06]

Shchekinov Y.A., Vasiliev E.O., 2004, A&A, 419, 19

Shchekinov Y.A., Vasiliev E.O., 2006, MNRAS, submitted (astro-ph/0604231)

Shull J. M., van Steenberg M. E., 1985, ApJ, 298, 268

Silk J., 1977, ApJ, 211, 638

Sommer-Larsen J., Dolgov A., 2001, ApJ, 551, 608

Spergel D. N. et al., 2006, ApJ, submitted (astro-ph/0603449)

Stasielak J., Biermann P. L., Kusenko A., 2006, ApJ, accepted (astro-ph/0606435)

Tegmark M., Silk J., Rees M. J., Blanchard A., Abel T., Palla F., 1997, ApJ, 474, 1 [T97]

White S.D.M., Rees M.J., 1978, MNRAS, 183, 341

Yoshida N., Abel T., Hernquist L., Sugiyama N., 2003, ApJ, 592, 645

Zaroubi S., Thomas R. M., Sugiyama N., Silk J., MNRAS, accepted, astro-ph/0609151

Zdziarski A. A., Svensson R., 1989, ApJ, 344, 551